Chemicals and Instruments

All buffers and chemicals were from Sigma-Aldrich unless otherwise stated. All water used was metal-free, ultrapure (>18.2 MΩ cm^{-1} at 25 °C), obtained by using Chelex 100 Resin (Bio-Rad). PD-10 columns were from GE Healthcare. ^{89}Zr-oxalate was provided by the Memorial Sloan Kettering Cancer Center (MSKCC) cyclotron and molecular imaging probe (CMIP) core. ^{89}Zr was produced on a TR19/9 cyclotron (Ebco Industries) via the ^{89}Y(p,n)^{89}Zr reaction and purified to yield ^{89}Zr with specific activities of 196-496 MBq/μg.

All instruments were calibrated and maintained in accordance with standard quality-control procedures. Activity measurements were performed using a CRC-15R dose calibrator (Capintec). Radioactive samples were counted in Automatic Wizard (2) γ-Counter (PerkinElmer). The radiolabeling of all scVEGF-DFO bioconjugates were monitored using salicylic acid impregnated instant thin-layer chromatography paper (iTLC-SA, Agilent Technologies) and analyzed on a Bioscan AR-2000 radio-TLC plate reader using Winscan Radio-TLC software (Bioscan Inc.). Bioluminescence experiments were performed using an IVIS spectrum fluorescence imaging system (PerkinElmer) and Living Image 4.4 software. The bioluminescent signal is expressed in photons per second and displayed as an intensity map. The image display is adjusted to provide optimal contrast and resolution in the image without affecting quantitation. All PET imaging experiments were conducted on a Focus 120 MicroPET camera (Siemens).

Cell Lines

293/KDR cells are derivatives of HEK293 human embryonic kidney cells (ATCC® CRL-1573™) engineered to overexpress VEGFR-2 receptor (*1*). 4T1luc cells are derivatives of 4T1 mouse mammary tumor cells (ATCC® CRL-2539™), engineered to stably express firefly luciferase (*1*). 293/KDR cells were cultured in DMEM media (Gibco® Cell Culture Media - Thermo Fisher Scientific) with non-essential amino acids, 10% fetal bovine serum and 1% penicillin/streptomycin

at 37 °C in a humidified atmosphere with 5% CO_2. Upon thawing, the cells were grown using DME HG (+ 10% FCS + 2mM L-Glutamine + Penicillin + Streptomycin) medium modified to contain 2 mM L-glutamine, 10 mM HEPES, 1 mM sodium pyruvate, 4500 mg/L glucose, and 1500 mg/L sodium bicarbonate, for use in incubators with 5% CO_2 in air. 4T1luc cells were grown using DME medium with 10% FCS + 2mM L-Glutamine + Penicillin + Streptomycin, 4500 mg/L glucose, and 3700 mg/L sodium bicarbonate, for use in incubators with 5% CO_2 in air. Cells were utilized in *in vivo* experiments after they reached 70-80% confluence.

Animal Model

All animal experiments within this study were performed in accordance with protocols approved by the Institutional Animal Care and Use Committee of MSKCC and followed National Institutes of Health guidelines for animal welfare.

For inoculation of mouse breast cancer carcinoma 4T1*luc* cells to the mouse mammary fat pad, mice were anesthetized with 1-2% isoflurane gas in medical air at a rate of 2 L/min. Surgery was performed on a heated platform to help maintain body temperature. After induction of anesthesia, the animal was weighed, and meloxicam (2.0 mg/kg) was administered perioperatively subcutaneously. The lower abdomen or chest area was shaved with electronic clippers. The surgical site was treated with a local intradermal infiltration of 0.25% bupivacaine solution applied with a 28–30G needle in 10 μl doses (100 μl in total) to the area surrounding the incision site. An 8–15 mm incision was made with sharp scissors or a scalpel at the level of the abdominal (4^{th} moving from cranial to caudal) and inguinal (5^{th}) nipples, or alternatively between the 2^{nd} and 3^{rd} thoracic nipples. The mammary fat pad was exposed by blunt dissection and exteriorized using fine forceps. The injection of $0.1–1.0\times10^6$ cells in medium was given into the mammary fat pad directing the tip of the needle laterally from the incision. The injection formed a bleb contained by the mammary fat pad. The mammary fat pad was carefully placed back into the subcutaneous space, and the incision was closed by one or two 9 mm autoclip-staples. For

tracer injections, Balb/c mice were anesthetized and the procedure was conducted as follows: For all intravenous injections, mice were gently warmed with a heat lamp and placed in a restrainer. The tails were sterilized with alcohol pads, and injection took place via the lateral tail vein.

Pan-receptor scVEGF and receptor-specific mutants of scVEGF

241-aa single-chain (sc) VEGF, combining two 3-112 fragments of human VEGF A cloned head-to-tail and fused to an N-terminal 15-aa cysteine-containing tag for site-specific payload conjugation was previously described (*1,4*). Receptor-specific mutants scVR1 and scVR2 that bind preferentially to VEGFR-1 and VEGFR-2, respectively, were engineered by introducing the amino acid substitutions in each VEGF fragment of scVEGF, as follows: scVR1, carries the I65A and I176A substitutions, while scVR2 harbors the D82S, G84M, LL85R, D193S, G195M, and L196R substitutions. The substitutions in similar positions in wild-type VEGF were previously described as creating significant specificity toward VEGFR-1 or VEGFR-2 (*2,3*). The DNA fragments encoding scVR1 and scVR2 were produced, confirmed by sequencing, and cloned in the pET29a(+) bacterial expression vector (Invitrogen), as service by GenWiz. Expression in E. Coli strain BL21(DE3), refolding, and purification of scVR1 and scVR2 proteins followed the protocols developed for scVEGF (*1,4*) with minor modifications, which will be published separately.

Site-specific conjugation of PEGylated DFO-chelators to targeting proteins

The ^{89}Zr-chelator deferoxamine (DFO) was conjugated to pan-receptor scVEGF or its receptor-specific mutants in a two-step procedure. First, NH_2-PEG (3.5 kDa)-maleimide (Jenkem Technology) was mixed 1.2-fold molar excess p-SCN-Bn-Deferoxamine (p-SCN-DFO, Macrocyclic) in DMSO in the presence of 4-6 molar equivalents of trimethylamine (Sigma-Aldrich). After 2 h of incubation at RT, unreacted p-SCN-DFO was quenched with 10-fold excess of Tris-

HCl pH 8.0 for 1h. In the second step, *de novo* synthesized reagent DFO-PEG-maleimide was mixed with [C4]-monothiol-scVEGF, or its mutants, to a final protein to maleimide molar ratio of 1:4 and incubated for 30 min at RT. To separate unreacted components, the reaction mixtures were then passed through PD10 columns (GE Healthcare) followed by either ion-exchange chromatography on Resource S column (GE Healthcare) for scVEGF and scVR1 conjugates, or RP-HPLC purification on C18 (YMC, Inc., USA), for scVR2 conjugate. The purity of the resulting conjugates, named scVEGF/DFO, scVR1/DFO, and scVR2/DFO, was analyzed by non-reducing SDS-PAGE on 15% PAAG gels and RP-HPLC. The conjugates, were dialyzed against 50 mM $(NH_4)HCO_3$, aliquoted at 5 nmol/vial (150 µg/vial), lyophilized, and stored at -80 ^{o}C.

Radiolabeling with ^{89}Zr

For radiolabeling reactions, lyophilized conjugates (1.5-5 nmol, 45-150 µg) were dissolved in 0.5 M HEPES pH 7.3 with concentrations of 1 mg/mL. ^{89}Zr-oxalate solution (30-130 MBq [0.8-3.5 mCi], 100-350 µL, pH = 6.6-6.8) was added to the conjugate solution and the mixture was incubated at 37˚C with agitation (600 rpm) for 1 h. ^{89}Zr-incorporation was determined using iTLC (mobile phase: 50 mM EDTA-solution). The crude reaction mixture was purified using gel-chromatography (PD-10 column, GE Healthcare) and the purity of radiolabeled conjugates was determined by iTLC (Supplemental Fig. S2). Finally, radiolabeled conjugates were obtained with 86-92% radiochemical yield (RCY) and specific activities ≥9.8 MBq/nmol (≥264 µCi/nmol), and purities >99%.

PET Imaging

PET imaging experiments were carried out on a microPET Focus 120 (Siemens). After the administration of the ^{89}Zr-labeled tracer (10.4 – 12.9 MBq/mouse [280-350 µCi]) in 150 µL sterile saline) via intravenous tail vein injection (t = 0). For blocking studies, tracer (3.4-4 µg) was mixed

with 35-fold excess of indicated “cold” protein (130-140 μg), scVEGF, scVR1, or scVR2. Anesthesia was maintained using 1.5% isoflurane/oxygen gas mixture and static scans were recorded at various time points with a minimum of 12 million coincident events (8-25 m total scan time). An energy window of 350-700 keV and a coincidence time window of 6 ns were used. Data were sorted into 2-dimensional histograms by Fourier re-binning, and transverse images were reconstructed by filtered back-projection into a 128 × 128 × 63 (0.72 × 0.72 × 1.3 mm) matrix. The image data were normalized to correct for non-uniformity of response of the PET, dead-time count losses, positron branching ratio, and physical decay to the time of injection but no attenuation, scatter, or partial-volume averaging correction was applied. Activity concentrations (percentage of dose per g of tissue [%ID/g]) were determined by conversion of the counting rates from the reconstructed (filtered back-projection) images. Maximum intensity projection (MIP) images were generated from 3-dimensional ordered subset expectation maximization reconstruction (3DOSEM). All of the resulting images were analyzed using ASIPro VM™ software.

Biodistribution Studies

For *ex vivo* acute biodistribution studies at selected time points (2, 6, 12, 24, and 48 h p.i.), tracer (1-1.5 MBq/mouse [27-40 μCi]) was injected via the lateral tail vein. For blocking studies, tracer (1.4-1.6 μg) was mixed with 35-fold excess of indicated “cold” protein (49-56 μg), scVEGF, scVR1, or scVR2. Animals (n = 4/time point) were subsequently euthanized at the appropriate time points by CO_2 asphyxiation. After euthanization, tumor, nine major organs, and tissue samples from bone, skin, and muscle were harvested from euthanized mice, blotted with paper, dried in open air for 5 minutes, and placed into pre-weighed tubes and subsequently counted on the gamma-counter.

Dosimetry

Biodistribution data obtained from the utilized mouse model were first expressed as normal-organ mean standard uptake values (SUVs) versus time post-injection. Assuming, in first order, that SUVs are independent of body mass and thus the same among species, the mean SUV in mouse organ i, SUV_i, was converted to the fraction of the injected dose in each human organ I, FID_I, using the following formula and the organ and total-body masses of the 70-kg Standard Man anatomic model (*5*):

$$FID_I = SUV_i \bullet \frac{MassofHumanOrgan_I}{MassofHumanTotalBody}$$

These data (corrected for radioactive decay) were fit to exponential time-activity functions. The cumulated activity, or residence time, in human organ i (t_i, in μCi-h/μCi) was calculated by integrating the time-activity function in organ i, replacing the biological clearance constant, $(l_b)_x$ for each component, x, of the fitted exponential function with the corresponding effective clearance constant, $(l_e)_x$ [$(l_e)_x = (l_b)_x + l_p$, where l_p is the physical decay constant of the radionuclide] (*6*). The resulting organ residence times were entered into the OLINDA computer program to yield the mean organ absorbed doses and effective dose in rad/mCi and rem/mCi, respectively.

Immunohistochemistry

The Molecular Cytology Core Facility at MSKCC prepared slides with tumor tissue for histochemistry and immunohistochemistry. Harvested 4T1luc tumors were fixed in 10% formalin for 48 h, rinsed in PBS, and embedded in paraffin and cut to 5-μm sections that were subsequently subjected to H&E staining (hematoxylin–eosin) for white light microscopy. To unmask biomarkers, sections were de-waxed and incubated in 10 mM sodium citrate pH 6, 0.05% Tween-20 at 95 ^{o}C for 30 min. Double fluorescent staining with tyramine amplification technique was performed as described in details recently (*7*), with the following primary antibodies. For formalin-fixed tissue, VEGFR-2-specific (Cell Signaling #2479BC), VEGFR-1-specific (Abcam N-terminal-specific #Ab32152), and CD31-specific (DiaNova #DIA-310-M) antibodies were used. Slides were

mounted in medium for fluorescence with DAPI for nuclear counterstaining (Vector Laboratories) and observed in Zeiss Axiovert microscope. For quantitative analyses of immunofluorescent staining, digital images of multiple microscopic fields were obtained under identical conditions and the percentage of pixels containing antigen-specific staining above the same threshold for a selected region of interest was determined by histogram analysis using Zeiss software.

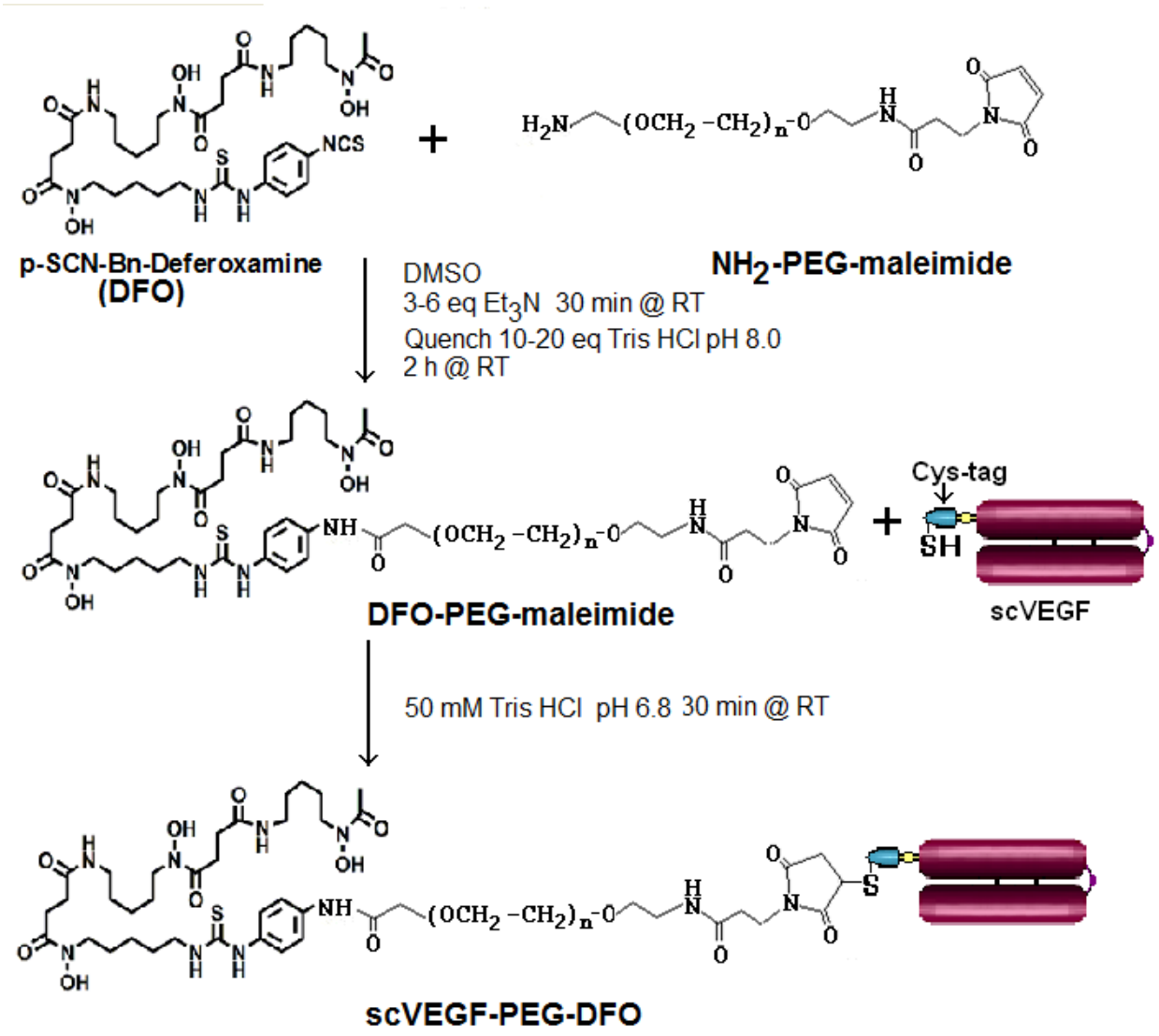

Supplemental Figure 1. Preparation of DFO conjugates.

A **B**

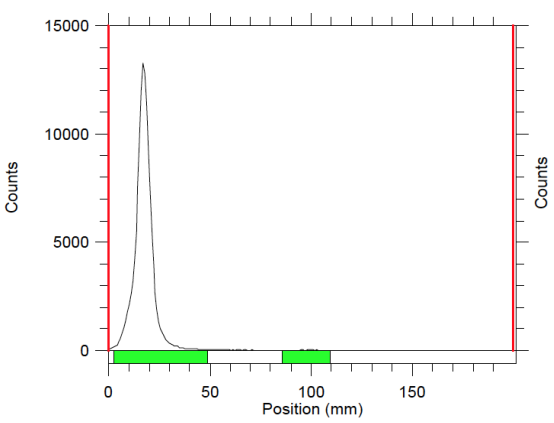

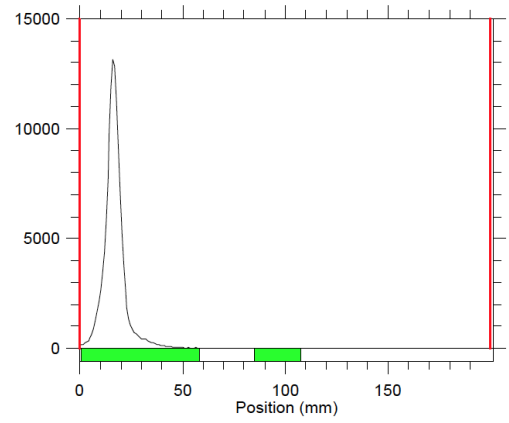

Reg	(mm) Start	(mm) Stop	(mm) Centroid	RF	Region Counts	Region CPM	% of Total	% of ROI
Rgn 1	2.5	48.7	17.4	0.087	129094.0	129094.0	98.49	99.64
Rgn 2	85.6	109.5	97.4	0.487	468.0	468.0	0.36	0.36
2 Peaks					129562.0	129562.0	98.85	100.00

Reg	(mm) Start	(mm) Stop	(mm) Centroid	RF	Region Counts	Region CPM	% of Total	% of ROI
Rgn 1	0.7	58.1	16.9	0.085	131188.0	787128.0	99.35	99.85
Rgn 2	84.7	107.8	96.2	0.481	201.0	1206.0	0.15	0.15
2 Peaks					131389.0	788334.0	99.50	100.00

C

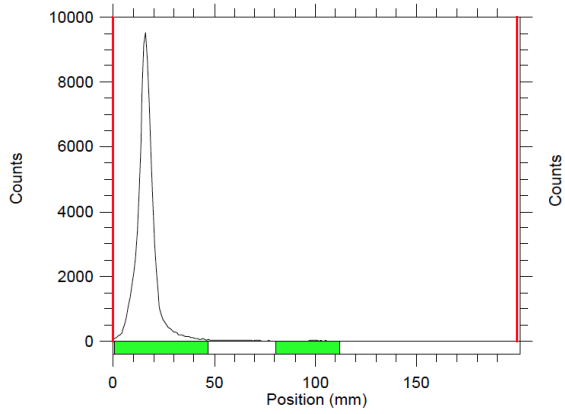

D

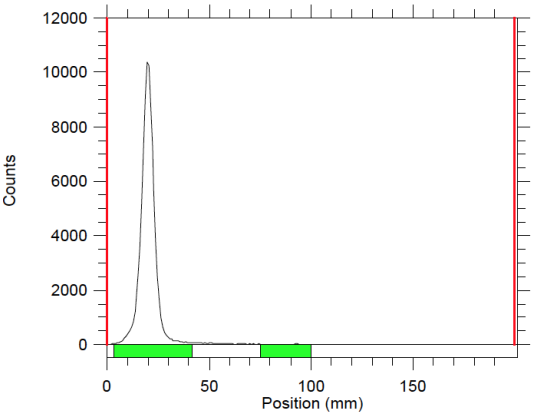

Reg	(mm) Start	(mm) Stop	(mm) Centroid	RF	Region Counts	Region CPM	% of Total	% of ROI
Rgn 1	3.3	41.9	20.1	0.100	88456.0	98284.4	98.03	99.71
Rgn 2	75.3	100.1	87.7	0.438	261.0	290.0	0.29	0.29
2 Peaks					88717.0	98574.4	98.32	100.00

Reg	(mm) Start	(mm) Stop	(mm) Centroid	RF	Region Counts	Region CPM	% of Total	% of ROI
Rgn 1	0.7	47.0	16.5	0.082	92209.0	553254.0	98.41	99.55
Rgn 2	80.4	112.1	94.6	0.473	415.0	2490.0	0.44	0.45
2 Peaks					92624.0	555744.0	98.86	100.00

E

F

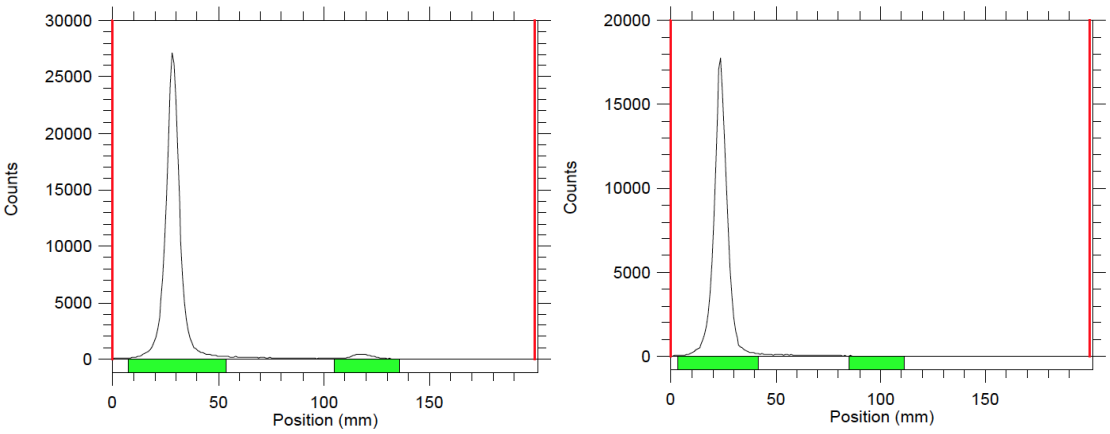

Reg	(mm) Start	(mm) Stop	(mm) Centroid	RF	Region Counts	Region CPM	% of Total	% of ROI
Rgn 1	7.6	53.9	28.8	0.144	244598.0	667085.5	94.55	97.37
Rgn 2	105.3	136.1	118.2	0.591	6606.0	18016.4	2.55	2.63
2 Peaks					251204.0	685101.8	97.10	100.00

Reg	(mm) Start	(mm) Stop	(mm) Centroid	RF	Region Counts	Region CPM	% of Total	% of ROI
Rgn 1	3.3	41.9	23.7	0.119	152726.0	366542.4	97.34	99.75
Rgn 2	84.7	111.3	94.0	0.470	377.0	904.8	0.24	0.25
2 Peaks					153103.0	367447.2	97.58	100.00

Supplemental Figure 2. iTLC analysis of ^{89}Zr-incorporation into protein conjugate in the reaction mixtures and quality control runs after tracer purification for scV/Zr (**A, B**), scVR1/Zr (**C, D**), and scVR2/Zr (**E, F**). The precursors, scV/DFO, scVR1/DFO, and scVR2/DFO were labeled using identical conditions and methods for characterization, as described in the methods section. ^{89}Zr-incorporation was monitored using salicylic acid impregnated iTLC plates and EDTA-solution (50 mM, pH = 6.8) as mobile phase. The radiolabeled protein conjugates remained near start point (Rgn 1) due to multiple charges within the protein structure, while remaining free $^{89}Zr^{4+}$ (captured by added EDTA) migrates with the solvent front (Rgn 2).

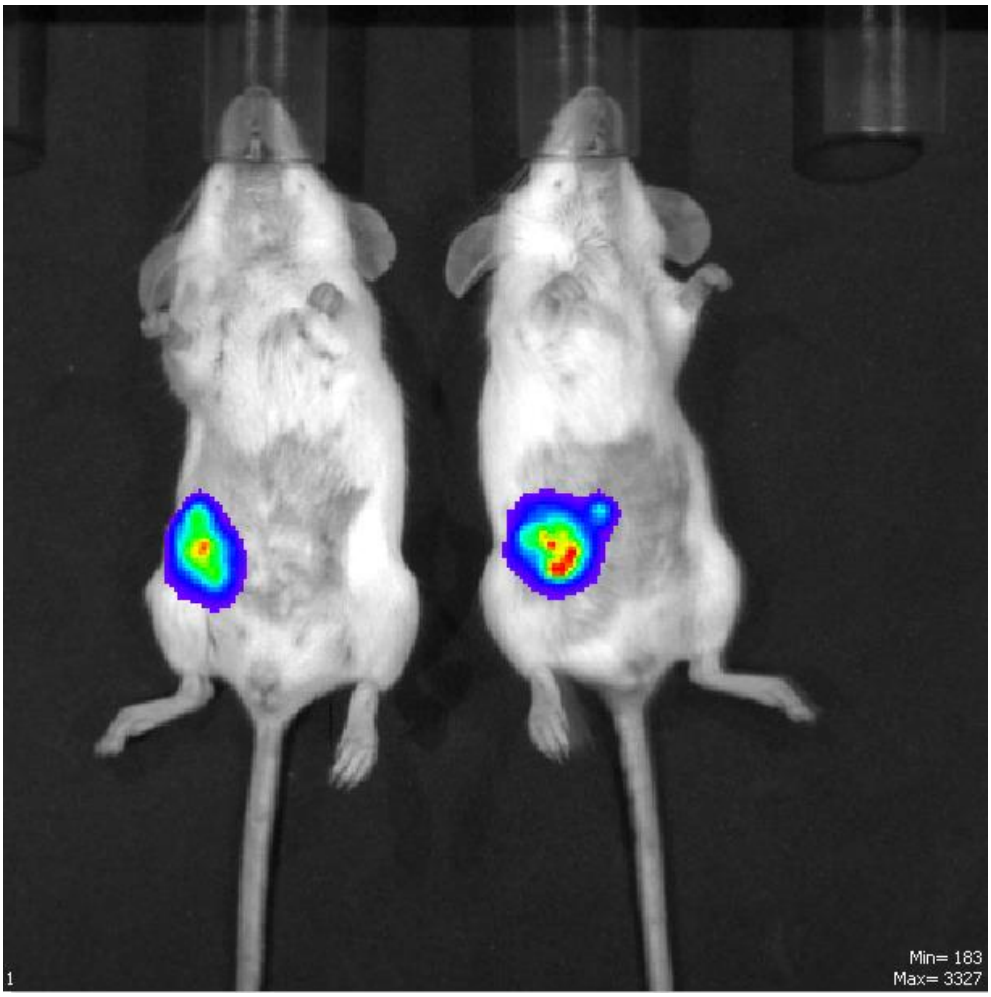

Supplemental Figure 3. Bioluminescent imaging of orthotopic 4T1*luc* tumors.

A

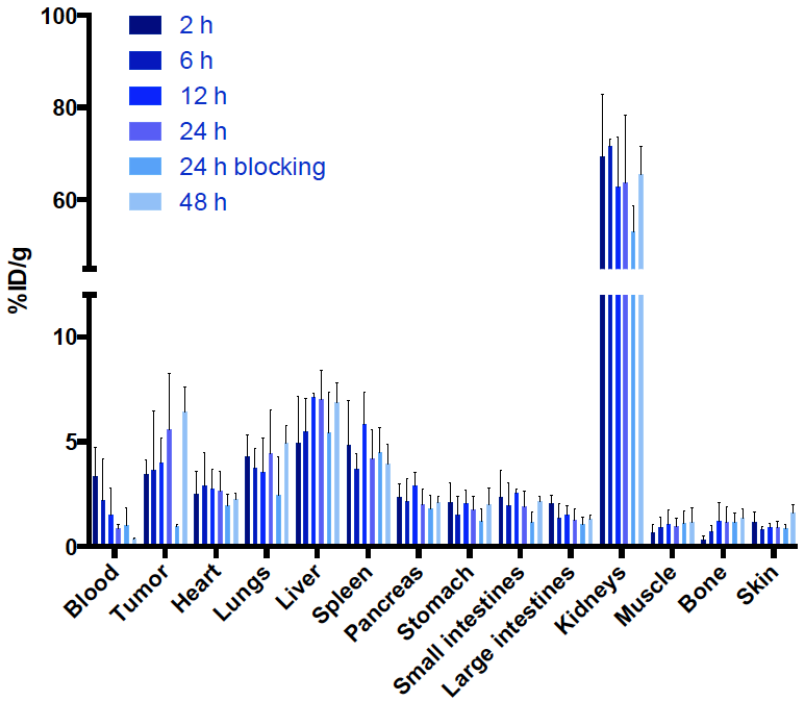
100
80
60
10
5
0
%ID/g
2 h
6 h
12 h
24 h
24 h blocking
48 h
Blood
Tumor
Heart
Lungs
Liver
Spleen
Pancreas
Stomach
Small intestines
Large intestines
Kidneys
Muscle
Bone
Skin

B

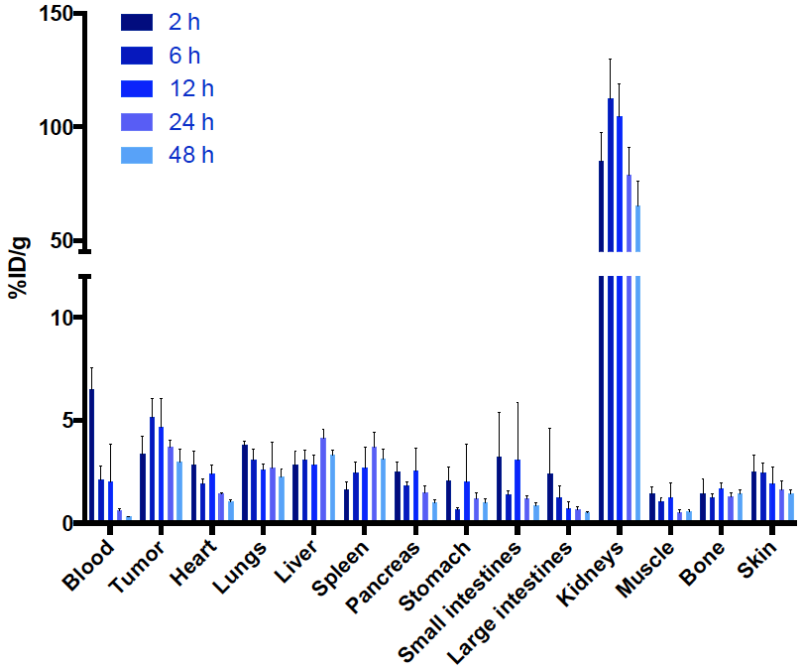
150
100
50
10
5
0
%ID/g
2 h
6 h
12 h
24 h
48 h
Blood
Tumor
Heart
Lungs
Liver
Spleen
Pancreas
Stomach
Small intestines
Large intestines
Kidneys
Muscle
Bone
Skin

C

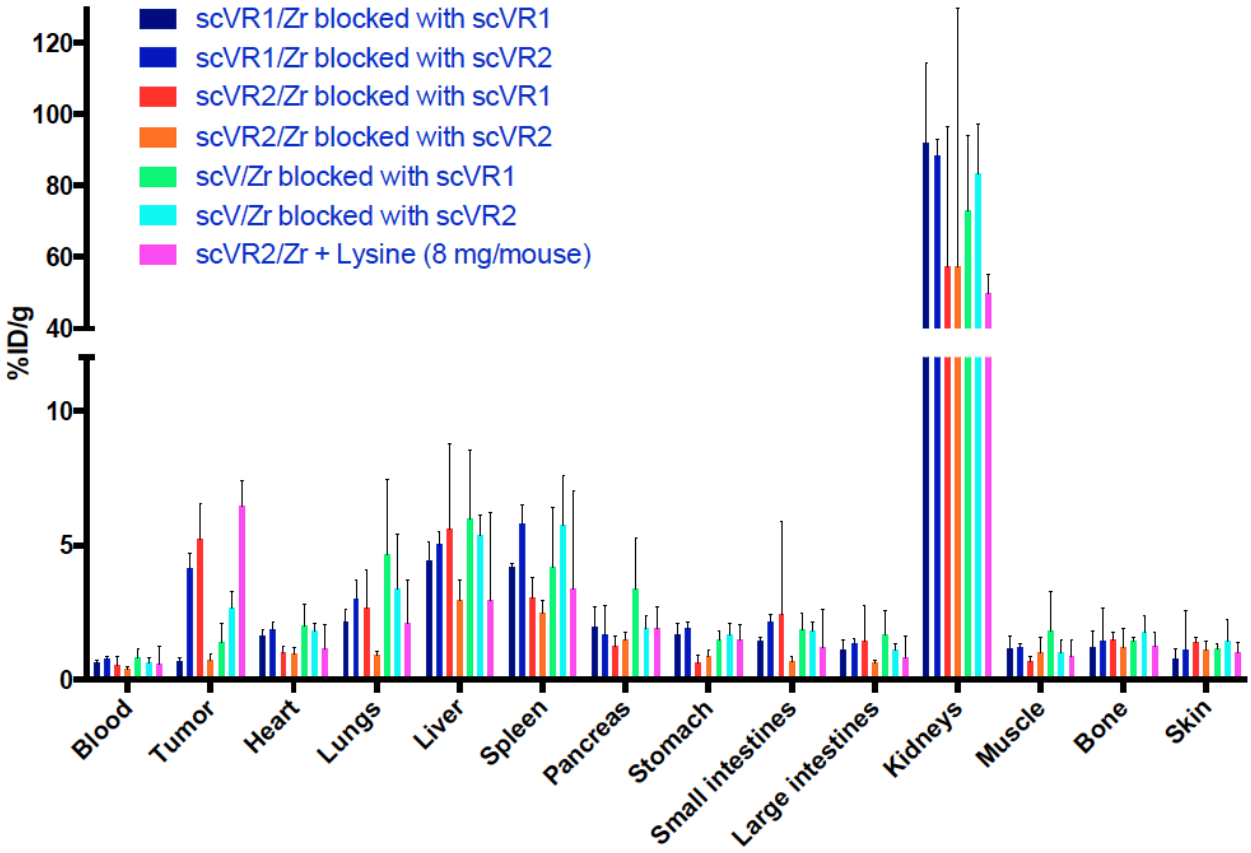

Supplemental Figure 4. Displayed are the *ex vivo* biodistribution data of scVR2/Zr (**A**) and scV/Zr (**B**) in major organs, as well as the full biodistribution study (**C**) of the blocking study for receptor-specificity determination. 4T1luc tumor-bearing Balb/c mice (n = 4/time point in each group) were injected 1-1.5 MBq/mouse of either scVR2/Zr (**A**), or scV/Zr (**B**) and the full blocking study (**C**). For blocking experiments, a 35-fold excess of “cold” scVEGF, or scVR1 or scVR2 was added to corresponding tracers prior to injection.

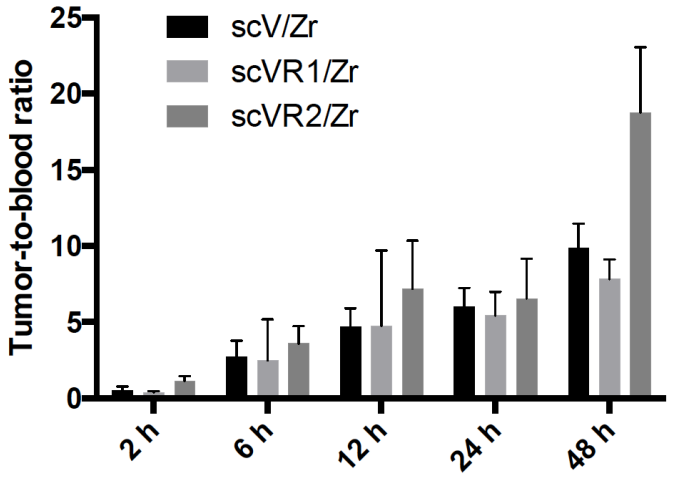

Supplemental Figure 5. Tumor-to-Blood ratios of all three tracers at the appropriate imaging and biodistribution time points. Due to the short blood half-life of the constructs (>2 h) increasing tumor-to-blood ratios were observed for all three tracers.

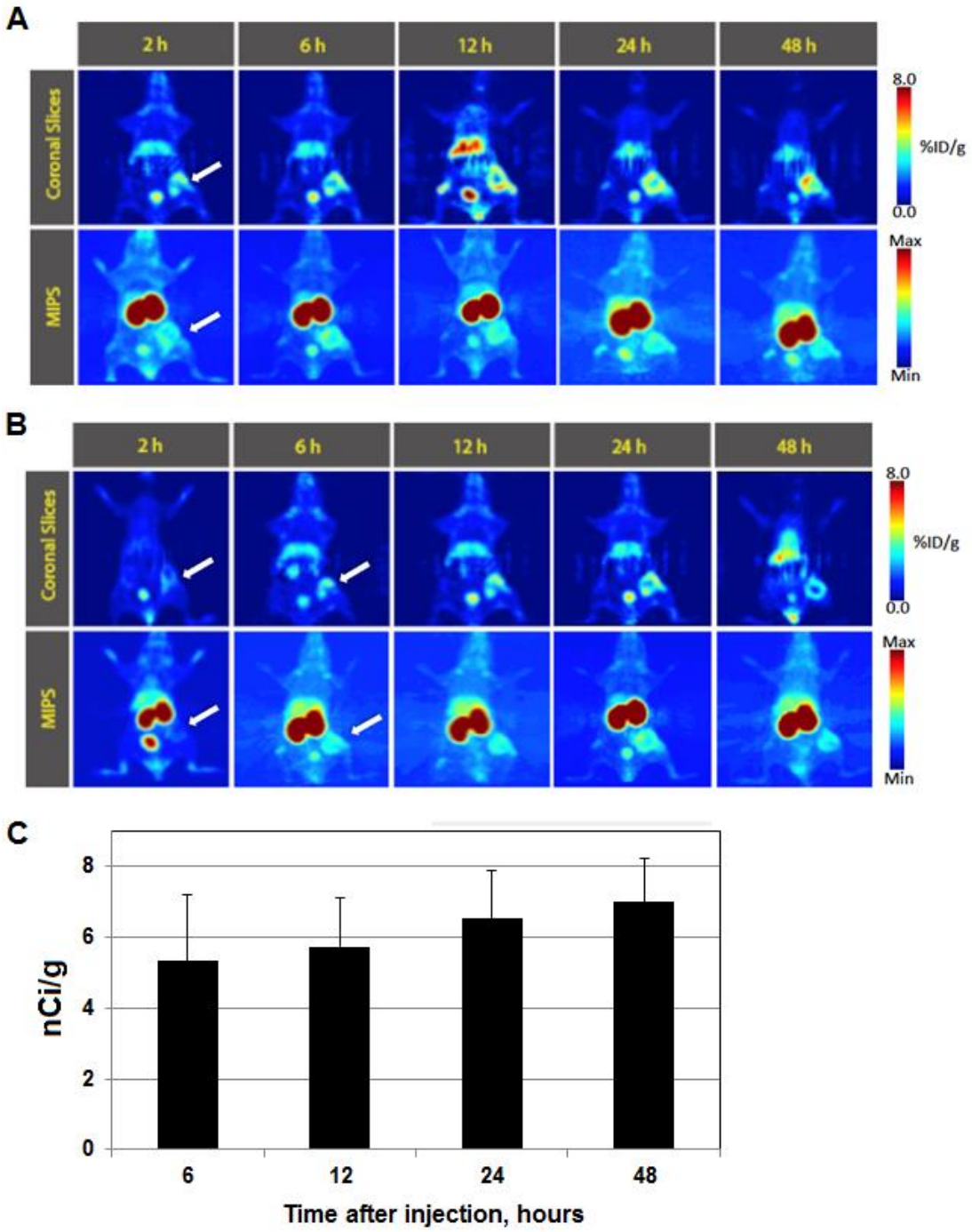

Supplemental Figure 6. **Longitudinal PET Imaging experiments. A**, scVR2/Zr, **B**, scV/Zr. For each tracer, coronal slices (Top) and maximum intensity projections (MIPs, bottom) are shown for the various imaging time points. **C**, time-dependent changes in %ID/g for scVR2/Zr, as determined from longitudinal imaging was in accordance with *ex vivo* biodistribution data.

Target Organ	scV/Zr	scVR1/Zr	scVR2/Zr
Adrenals	1.9	1.9	1.86
Brain	1.14	1.15	1.13
Breasts	0.941	0.953	0.93
Gallbladder Wall	1.66	1.51	1.5
LLI Wall	1.39	1.21	1.13
Small Intestine	1.59	1.42	1.37
Stomach Wall	1.76	1.35	1.33
ULI Wall	1.47	1.29	1.26
Heart Wall	1.25	1.09	1.07
Kidneys	11.2	10.7	10.7
Liver	1.55	1.56	1.81
Lungs	0.975	0.987	1.03
Muscle	1.02	1.07	0.933
Ovaries	1.4	1.43	1.34
Pancreas	1.81	1.81	1.77
Red Marrow	1.26	1.16	1.1
Osteogenic Cells	1.65	1.26	1.19
Skin	0.811	0.828	0.779
Spleen	1.7	1.7	1.7
Testes	1.07	1.1	1.01
Thymus	1.11	1.14	1.07
Thyroid	1.13	1.16	1.07
Urinary Bladder Wall	1.34	1.22	1.11
Uterus	1.46	1.33	1.16
Total Body	1.21	1.24	1.25
Effective Dose (rem/mCi)	**1.28**	**1.29**	**1.43**

Supplemental Table 1. Expected human dosimetry for all three tracers. Mean organ absorbed doses and effective doses calculated for all three ^{89}Zr-labeled scVEGF tracers given in rad/mCi and rem/mCi, respectively.

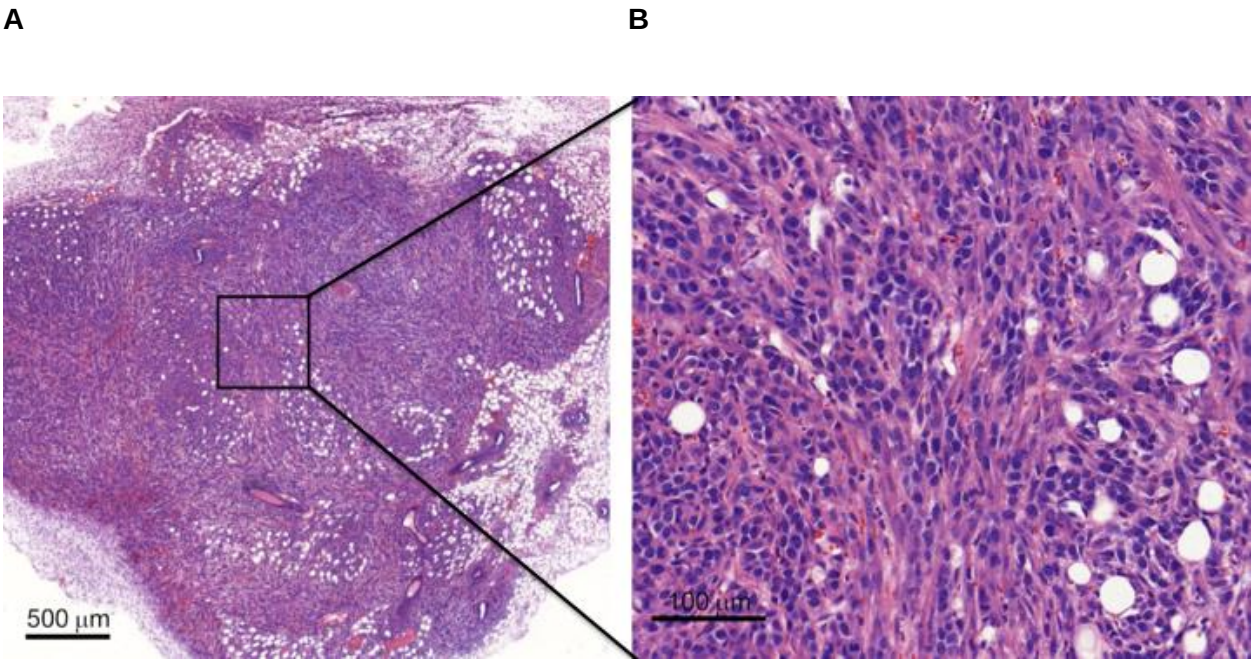

Supplemental Figure 7. H&E staining of 4T1luc tumor. Most of the tumor tissue consists of viable cells without a necrotic center (**A,** scale bar: 500 µm, magnification **B,** scale bar: 100 µm). This led to the conclusion that tracer uptake in the angiogenic rim is due to increased vasculature in the periphery of the tumor.

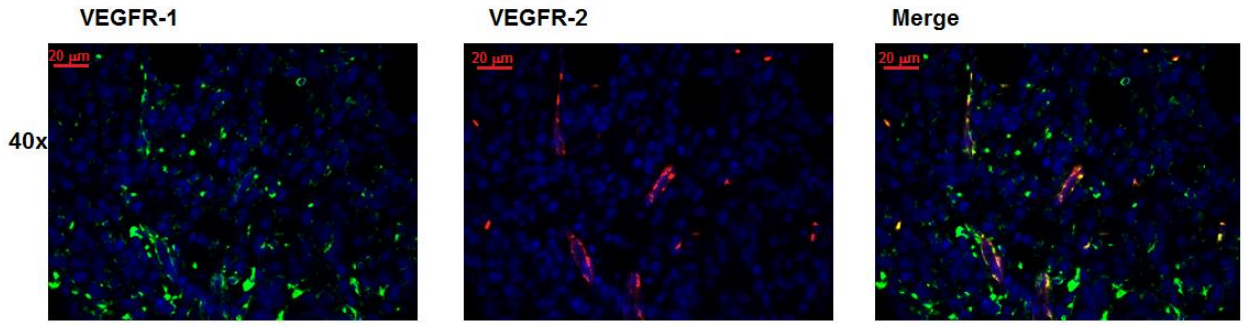

Supplemental Figure 8. Immunostaining for VEGFR-2 is colocalized with the subset of VEGFR-1 immunostaining. Double immunofluorescent staining for VEGFR-1 (green) and VEGFR-2 (red) in 4T1luc tumors. DAPI (blue), staining of nuclei. Magnification and scale bars are included. Note 1) higher prevalence of VEGFR-1 than VEGFR-2, and 2) virtually all VEGFR-2 is colocalized with VEGFR-1.

References

1. Backer MV, Levashova Z, Patel V, et al. Molecular imaging of VEGF receptors in angiogenic vasculature with single-chain VEGF-based probes. *Nat Med*. 2007;13:504-509.
2. Gille H, Kowalski J, Li B, LeCouter J, et al. Analysis of biological effects and signaling properties of Flt-1 (VEGFR-1) and KDR (VEGFR-2). A reassessment using novel receptor-specific vascular endothelial growth factor mutants. *J Biol Chem*. 2001;276:3222-30.
3. Li B, Fuh G, Meng G, et al. Receptor-selective variants of human vascular endothelial growth factor. Generation and characterization. *J Biol Chem*. 2000;275:29823-8.
4. Backer MV, Patel V, Jehning BT, Claffey KP, Backer JM. Surface immobilization of active vascular endothelial growth factor via a cysteine-containing tag. *Biomaterials*. 2006;27:5452-58.
5. Perk LR, Stigter-van Walsum M, Visser GW, et al. Quantitative PET imaging of Met-expressing human cancer xenografts with 89Zr-labelled monoclonal antibody DN30. Eur J Nucl Med Mol Imaging. 2008;10:1857-67.
6. Cristy M, Eckerman K. Specific absorbed fractions of energy at various ages from internal photon sources (I-VII). Oak Ridge National Laboratory Report ORNL/TM- 8381/V1-7. Springfield, VA: National Technical Information Service, Department of Commerce; 1987.
7. Kato Y, Zhu W, Backer MV, Neoh CC, et al. Noninvasive imaging of liposomal delivery of superparamagnetic iron oxide nanoparticles to orthotopic human breast tumor in mice. Pharm Res. 2015;11:3746-55.